

Submitted to The Astrophysical Journal

POLARIMETRIC DETECTION OF EXOPLANETS TRANSITING T- AND L-BROWN DWARFS

Sujan Sengupta

*Indian Institute of Astrophysics, Koramangala 2nd Block, Bangalore 560 034, India;
sujan@iiap.res.in*

ABSTRACT

While scattering of light by atoms and molecules yields large amount of polarization at the B-band of both T- and L-dwarfs, scattering by dust grains in cloudy atmosphere of L-dwarfs gives rise to significant polarization at the far-optical and infra-red wavelengths where these objects are much brighter. However, the observable disk averaged polarization should be zero if the clouds are uniformly distributed and the object is spherically symmetric. Therefore, in order to explain the observed large polarization of several L-dwarfs, rotation-induced oblateness or horizontally inhomogeneous cloud distribution in the atmosphere is invoked. On the other hand, when an extra-solar planet of Earth-size or larger transits the brown dwarf along the line of sight, the asymmetry induced during the transit gives rise to a net non-zero, time dependent polarization. Employing atmospheric models for a range of effective temperature and surface gravity appropriate for T- and L-dwarfs, I derive the time dependent polarization profiles of these objects during transit phase and estimate the peak amplitude of polarization that occurs during the inner contact points of the transit ingress/egress phase. It is found that peak polarization in the range of 0.2-1.0% at I- and J-band may arise of cloudy L dwarfs occulted by Earth-size or larger exoplanets. Such an amount of polarization is higher than that can be produced by rotation-induced oblateness of even the rapidly rotating L-dwarfs. Hence, I suggest that time resolved imaging polarization should be a potential technique to detect transiting exoplanets around L-dwarfs.

Subject headings: radiative transfer — polarization — scattering — brown dwarfs — planets and satellites: detection — occultations

1. INTRODUCTION

Brown dwarfs are believed to be born like a star but fail to become a main- sequence star because they have masses sufficient to ignite deuterium burning but insufficient to enter into the hydrogen burning main sequence. Therefore, they inhabit the realm between the least massive

stars and the most massive planets. The source of the observed radiation is the gravitational potential energy during the formation and contraction phase. With the decrease in temperature of an individual brown dwarf, it progressively passes through spectral types ranging from late M through the L, T and Y sequences. Detailed reviews on the properties of brown dwarfs are given by Chabrier & Baraffe (2000); Burrows et al. (2001); Kirkpatrick (2005); Marley & Robinson (2015). Synthetic spectra of cloud-free model atmospheres fit well the observed spectra of field T dwarfs later than about type T4 because dust grains condensation takes place well below the photosphere and therefore are not an important opacity source (Stephens et al. 2009). On the other hand, inclusion of condensate cloud of various species such as iron, forsterite (Mg_2SiO_4), and enstatite (MgSiO_3) explains the spectra of L dwarfs (Cushing et al. 2008; Marley & Robinson 2015).

Similar to the case of the Sun and cool stars, thermal radiation of both T- and L- dwarfs should be linearly polarized at the near-optical wavelengths, e.g., in the B-band due to Rayleigh scattering by atoms and molecules. On the other hand, the presence of dust grains in the visible atmosphere of L-dwarfs gives rise to significant amount of linear polarization in the far-optical and in the infra-red regions. However, the net observable polarization would be zero if the object is spherically symmetric and the clouds are distributed uniformly. Linear polarization has been detected in the optical bands from a good number of L dwarfs covering almost the entire range of spectral types L0–L8 (Menard et al. 2002; Zapatero Osorio et al. 2005; Tata et al. 2009; Zapatero Osorio et al. 2011; Miles-Paez, Zapatero Osorio, Palle & Pena Ramirez 2013). Scattering by horizontally homogeneous clouds in the atmosphere of a rotation-induced oblate L-dwarf can explain the observed polarization. (Sengupta & Krishan 2001; Sengupta 2003; Sengupta & Kwok 2005; Sengupta & Marley 2010). Moreover, imaging polarimetric data of L dwarfs shows increase in the amount of polarization with the increase in spin rotation velocity (Miles-Paez, Zapatero Osorio, Palle & Pena Ramirez 2013) implying dominant role played by the asymmetry due to rotation-induced oblateness. However, in agreement with the analysis of Sengupta & Marley (2009), no polarization is detected from any T-dwarf to date.

Apart from the asymmetry that may arise due to rotation-induced oblateness of the stellar disk or/and horizontally inhomogeneous clouds in the atmosphere, asymmetry in the stellar disk can also be produced by a transiting planet that blocks the stellar disk partially. Consequently, transit of planet can also give rise to net non-zero disk integrated polarization. Such transit or occultation polarization of stars of different spectral types has been discussed in detail by a few authors (Carciofi & Magalhaes 2005; Wiktorowicz & Laughlin 2014; Kostogryz et al. 2011).

Giant exoplanets around brown dwarfs are discovered by direct imaging (Chauvin et al. 2004; Todorov, Luhman & Mcleod 2010), radial velocity method (Joergens & Muller 2007) and by gravitational microlensing method (Han et al. 2013). Recently a Venus-size planet has been discovered by microlensing (Udalsky et al. 2015). These discoveries clearly imply that formation of exoplanets with size ranging from Jovian to sub-Earth is possible around brown dwarfs either through binary star formation mechanism or through the scale-down core-accretion mechanism of planet formation

around a star. Therefore, a large number of exoplanets around brown dwarfs are awaiting to be detected. Discovery of these planets may highly populate the number of exoplanets because brown dwarfs together with M-dwarfs account for over 80 % of the stellar population of the Galaxy (Apai 2013). In fact, such a realization prompted to propose strategies for detecting habitable planets around brown dwarfs (Caballero & Rebolo 2002; Caballero 2010; Belu et al. 2013). However, as pointed out by Udalsky et al. (2015), owing to the limitation of available technology, substantially lower-mass planetary companions to brown dwarfs can only be discovered at present by using the gravitational microlensing technique.

In this paper, I show that time resolved image polarimetry can be a potential tool to detect planets transiting cloudy L-dwarfs. Using detailed atmospheric models for cloudy L-dwarfs, the scattering polarization is calculated and it is shown that the asymmetry induced by a transiting Earth-size planet gives rise to significant amount of disk-integrated linear polarization in both I- and J-bands at the inner contact points of transit ingress/egress phase that may be detected by the existing imaging polarimeters.

In the next section, I briefly describe the formalism adopted to estimate the time-resolved transit polarization profile of T- and L-dwarfs. In section 3, I discuss the results following by our conclusions in section 4.

2. METHOD FOR CALCULATING THE TRANSIT POLARIZATION

The net polarization of the star during the transit is calculated by multiplying the intensity and scattering polarization at each radial point along the stellar disk with the fractional circumference occulted by the projection of the planet over the surface of the star. The disk-averaged polarization during the transit phase or the transit polarization is given by Sengupta & Marley (2016); Wiktorowicz & Laughlin (2014); Carciofi & Magalhaes (2005). Here we use the formalism presented in Sengupta & Marley (2016). Accordingly,

$$p(t) = \frac{1}{F} \int_{r_1}^{r_2} 2 \sqrt{\frac{[(1 - \mu^2)^{1/2} - r_m(t)]^2 - w^2}{1 - \mu^2}} I(\mu) P(\mu) \mu d\mu, \quad (1)$$

where F is the flux of the unobscured star, $I(\mu)$ and $P(\mu)$ are the specific intensity and polarization respectively along μ , $\mu = \cos \theta = \sqrt{1 - r^2}$ with θ being the angle between the normal to the planetary surface and the line of sight and r being the radial points along the stellar disk, $0 \leq r \leq 1$, $r_1 = \sqrt{1 - [r_m(t) + w]^2}$ and $r_2 = \sqrt{1 - [r_m(t) - w]^2}$, $r_m(t)$ is the instantaneous position of the center of the planet and is given by

$$r_m(t) = \left[b^2 + 4 \{ (1 + w)^2 - b^2 \} \left(\frac{t}{\tau} \right)^2 \right]^{1/2}. \quad (2)$$

In the above expression, the impact parameter b for a circular orbit of radius a is given by $b = a \cos i / R_\star$, where i is the orbital inclination angle of the planet and R_\star is the stellar radius, $w =$

R_P/R_\star is the ratio of the planetary radius (R_P) to the stellar radius. The transit duration τ is given by Scharf (2009)

$$\tau = \frac{P}{\pi} \sin^{-1} \left[\frac{R_\star}{a} \left\{ \frac{(1+w)^2 - b^2}{1 - \cos^2 i} \right\}^{1/2} \right] \quad (3)$$

and t is the time since mid-transit. Transit of planet can occur only if the inclination angle $i \geq \cos^{-1} \left(\frac{R_\star + R_P}{a} \right)$.

In order to calculate the specific intensity $I(\mu)$ and scattering polarization $P(\mu)$, I have employed one-dimensional, non-grey, hydrostatic and radiative-convective atmospheric models for a range of effective temperature T_{eff} and surface gravities g appropriate for L- and T-dwarfs (Ackerman & Marley 2001; Marley et al. 2002; Freedman et al. 2008; Saumon & Marley 2008). For T-dwarfs, cloudless model atmosphere generally reproduce the spectra of most T dwarfs with $T_{\text{eff}} < 1200 - 1300$ K (Stephens et al. 2009). In the present work, I consider cloudless models for T-dwarfs appropriate for spectral types later than about T3 (Stephens et al. 2009). However, condensates are included in the chemical equilibrium calculation (Freedman et al. 2008). For T-dwarfs, I choose models with $T_{\text{eff}} = 1300, 1100, 900$, and 700 K for a fixed value of $g=1000 \text{ ms}^{-2}$.

For the relatively hotter L-dwarfs, spatially uniform dust cloud is included. The efficiency of sedimentation of cloud particles in the atmospheric models is controlled through a scaling factor f_{sed} . In the present work I adopt $f_{\text{sed}} = 2.0$ (Cushing et al. 2008; Stephens et al. 2009). For L-dwarfs, I choose models with $T_{\text{eff}} = 1400, 1600, 1800, 2000$ and 2200 K for two different values of $g=300$ and 1000 ms^2 . The atmosphere model employed here fits the spectra and photometry of a large number of brown dwarfs at a wide range of wavelengths covering near optical to mid-infrared regions.

The two Stokes parameters I and Q are calculated in a locally plane-parallel medium by solving the vector radiative transfer equations. For the cloudy L-dwarfs, the angular distribution of the photons before and after scattering is calculated by using a combined Henyey-Greenstein-Rayleigh phase matrix (Liu & Weng 2006) while for T-dwarfs, Rayleigh phase matrix is sufficient (Chandrasekhar 1960). The detailed formalisms as well as the numerical methods for calculating the angle dependent total and polarized intensity I and Q are described in Sengupta & Marley (2009). In fact, in order to calculate the transit or occultation polarization profiles presented here, I have used the same values of $I(\mu)$ and $P(\mu)$ that are used in Sengupta & Marley (2009) for T-dwarfs and in Sengupta & Marley (2010) for L-dwarfs.

I have fixed the orbital separation a between the brown dwarfs and the exoplanets at 0.01 AU and have calculated the orbital period P by using Kepler's law. The radius of the brown dwarf is fixed at $1R_J$ where R_J is the radius of Jupiter. The mass of the brown dwarf is calculated from its surface gravity. It must be emphasized here that this is just a representative case. The amount of polarization originated due to transit is not affected by the orbital distance or period but it determines the interval between the two successive amplitudes of polarization that occur at the inner contact points of the transit ingress/egress phase.

3. RESULTS AND DISCUSSIONS

The center-to-limb variation in the polarization across any stellar disk arises due to the scattering albedo which is determined by the contribution of scattering opacity to the total opacity in the atmosphere (Harrington 1969). The polarization is zero at the center ($\mu = 1$) of the stellar disk and is maximum at the limb ($\mu = 0$). Linear polarization in cool stars including T dwarfs arises by scattering of light with atoms and molecules and the maximum amount of polarization that occurs at the stellar limb is usually very small. Polarization for solar type stars varies from a few times of 10^{-4} near the limb to a few times of 10^{-6} near the center (Fluri & Stenflo 1999) at near-optical (B-band) wavelengths. At longer wavelengths, the polarization is extremely small. The scattering polarization of cloudless T-dwarfs does not differ significantly from that of a cool star but large amount of polarization in longer wavelengths arises due to dust scattering in cloudy L dwarfs.

As mentioned earlier, in the absence of clouds in the visible atmosphere, the polarization of T-dwarfs arises due to Rayleigh scattering by atoms and molecules. Therefore the largest amount of polarization arises at shorter wavelengths. Figure 1 presents the B-band transit or occultation polarization of T-dwarfs with different effective temperatures. For a fixed surface gravity, the gas density increases with the decrease in T_{eff} and hence the scattering probability increases yielding into higher polarization. It is worth mentioning that the amount of polarization is determined by the atmospheric models invoked.

The double peaked polarization profile, a general feature of transit polarization of any star, arises because of the fact that the maximum polarization occurs near the inner contact points of transit ingress/egress phases. For central transit i.e., when the inclination angle $i = 90^\circ$, the projected position of the center of the planet coincides with the center of the star during mid transit. This gives rise to a symmetry to the projected stellar disk. Hence the disk integrated polarization for central transit is zero during mid transit. Owing to increase in asymmetry to the stellar disk, the polarization increases as the planet moves from the center ($t = 0$) to the limb ($t = \pm\tau/2$) of the stellar disk. However, when the eclipse is off center, i.e., when $i \leq 90^\circ$, the polarization is non-zero during the whole transit epoch including the mid transit time. Nevertheless, the peak polarization is independent of the orbital inclination angle but depends on the ratio of the planetary to stellar radii.

As presented in figure 1, for an Earth-size transiting planet, the B-band peak polarization at the inner contact points of transit ingress/egress phase is 0.06% for T-dwarfs with $T_{\text{eff}} = 700\text{K}$. The peak polarization becomes about 0.12% when the size of the transiting planet is three times the size of the Earth. The asymmetry in the stellar disk increases with the increase in the ratio between the planetary and stellar radii and hence the disk-integrated polarization increases. The transit duration depends on the size of both the star and the planet, on the orbital distance of the planet from the star and on the orbital inclination angle. Therefore, for a given orbital distance, the peak polarization occurs at different time for different size ratio and inclination angle.

The transit polarization of T-dwarf is maximum at B-band and the peak polarization is very small, between 0.02 to 0.06 % for an Earth-size transiting planets. Since the object is also faint at near-optical, detecting such low polarization could be challenging. It's worth mentioning here that B-band polarimetric observation of brown dwarfs is not reported till date and no polarization is detected for any T-dwarf at longer wavelengths (Jensen-Clem et al. 2016).

On the other hand, formation of dust grains in the cloudy atmosphere of L brown dwarfs provides an additional scattering opacity to the gas opacity. The thermal radiation of the cloudy L dwarfs is polarized by dust scattering giving rise to large value of limb polarization in the far-optical and infra-red wavelengths. Figure 2 presents the J-band transit polarization of L-dwarfs. Although the overall feature of the transit polarization profile remains the same to that of T-dwarfs at B-band, the degree of polarization increases by several times at J-band. As demonstrated by Sengupta & Marley (2010); Marley & Sengupta (2011), the degree of polarization of cloudy L dwarfs and self-luminous exoplanets depends on the effective temperature and the surface gravity of the objects. The scattering opacity is determined by a balance between the downward transport by sedimentation and upward turbulent diffusion of condensates and gas and hence the polarization varies with different effective temperature and surface gravity. Figure 2 shows that L-dwarfs of mid-spectral type corresponding to $T_{\text{eff}} = 1600 - 1800\text{K}$ produce the largest amount of polarization at the inner contact points of transit ingress/egress phase when the surface gravity $g=1000 \text{ ms}^{-2}$. Polarization reduces with the decrease in surface gravity and effective temperature. At the same time, for a given surface gravity polarization reduces when the effective temperature of the object rises above 1800 K. An increase in temperature causes the cloud base to shift upward yielding a smaller column of dust grains in the observed atmosphere and hence the polarization decreases with the increase in effective temperature.

Although the scattering polarization is sensitive to the effective temperature and the surface gravity, the amount of transit polarization strongly depends on the asymmetry in the stellar disk produced during the transit phase. This asymmetry is governed by the size of the transiting planet as compared to the size of the L dwarf. In the present work, I have adopted a Jupiter size L-dwarf. Figure 3 presents the transit polarization at I- and J-bands of a L-dwarf with fixed surface gravity and effective temperature but for different sizes of the transiting planet. As the asymmetry increases with the increase in the size of the transiting planet, the amount of polarization at the inner contact points of the ingress/egrees phase increases linearly. Figure 3 also indicates that the amount of polarization in J-band is higher than that in I-band. In fact, the peak amplitude of polarization in J-band is almost double to that in I-band. The adopted cloud model, e.g., the size distribution, the number density of the dust grains as well as the location of the cloud base and deck dictates the amount of polarization at different wavelengths.

As mentioned before, the orbital inclination angle of the transiting planet does not determine the amount of polarization at the inner contact points of the transit ingress/egress phase but affects the time interval between the two successive peaks of polarization. Figure 4 shows the J-band transit polarization due to a transiting planet having different orbital inclination angles.

As the inclination angle decreases from its maximum value of 90° , the transit path of the planet shifts towards the edge of the star shortening the transit period. The amount of polarization at the mid transit ($t=0$) increases with the decrease in the inclination angle. As the distance between the inner contact points of the ingress and the egress phase shortens, the time interval between the occurrence of the two polarization peaks reduces and subsequently the two peaks merge into one central peak when the inclination angle attains its minimum value beyond which a full transit is not possible. This is consistent with the results presented by Carciofi & Magalhaes (2005) for solar type of stars. A partial transit however, reduces the degree of disk integrated polarization.

The amount of polarization at the inner contact points of transit ingress/egress phase clearly implies that the asymmetry produced by an Earth-size transiting planet can be higher than that caused by rotation-induced oblateness of brown dwarfs. Although, rotation-induced oblateness explains the observed I-band polarization of many L-dwarfs, the required asymmetry needs a surface gravity lower than 1000 ms^{-2} (Sengupta & Marley 2010). The surface gravity of brown dwarfs, although is poorly constrained by their spectra, some L dwarfs show such a large polarization that it can be explained only if the spin rotation velocity is extremely high. For example, the observed degree of polarization 2MASS J2158-1550 (L4.0) and 2MASS J1807+5015 (L1.5) are 1.38 % and 0.7% respectively and so a spin rotation velocity of more than 100 kms^{-1} is required to explain such high polarization. On the other hand, I-band polarization of 2.45% observed from 2MASS J2244+2043 (L6.5) remains unexplained. None of these L dwarfs showed optical variability and hence rules out high inhomogeneity in atmospheric cloud distribution. Transit by a Neptunian planet may explain such high polarization. Time resolved imaging polarimetry may verify such a possibility.

4. CONCLUSIONS

Assuming the transit of an exoplanet around cloudy L-dwarfs and cloudless T-dwarfs, I have presented the transit polarization profiles of brown dwarfs and estimated the peak polarization at the inner contact points of transit ingress/egress phase for a large number of model atmospheres and planetary radii. For this purpose, the atmospheric models that fit the observed spectra of L and T-dwarfs are employed. The B-band linear polarization due to scattering by atoms and molecules in the atmosphere of T-dwarfs and I- and J-bands linear polarization due to scattering by dust grains in the atmosphere of L-dwarfs are calculated numerically. Our investigation implies that detectable amount of transit polarization may arise in both I- and J-bands of a cloudy L-dwarf if an Earth-size or larger planet transits it giving rise to asymmetry in the stellar disk. However, the transit polarization of the cloudless T dwarfs is found to be too small to be detected. Therefore, it is suggested that time resolved image polarimetry could be a potential tool to detect planets around L dwarfs.

Our model estimations imply that for L dwarfs with spectral types ranging from L3 to L7, the peak polarization at the inner contact points of the transit ingress/egress phase should be 0.5-1.0%

in J-band and 0.2-0.5% in the I-band for transiting planets of size $1 - 3R_{\oplus}$. Such an amount of polarization can easily be detected by several existing facilities including FORS1 onboard VLT.

REFERENCES

- Ackerman, A. & Marley, M. S. 2001, *ApJ*, 556, 872.
- Apai, D. 2013, *Astron.Nachr.* 334, 57
- Belu, A. R., Selsis, F., Raymond, S. N. et al. 2013, *ApJ*, 768, 125
- Burrows, A., Hubbard, W. B., Lunine, J. I., & Liebert, J. 2001, *Rev. Mod. Physics*, 73, 719
- Caballero, J. A. 2010, *Highlights of Spanish Astrophysics V, Astrophysics and Space Science Proceedings* (Berlin: Springer), 79
- Caballero, J. A., & Rebolo, R. 2002, in *First Eddington Workshop on Stellar Structure and Habitable Planet Finding*, ed. F. Favata, I. W. Roxburgh, & D. Galad Enr quez (ESA SP-485; Noordwijk: ESA), 261
- Carciofi, A. C., & Magalhaes, A. M. 2005, *ApJ*, 635, 570
- Chabrier, G., & Baraffe, I. 2000, *ARA&A*, 38, 337.
- Chandrasekhar, S. 1960, *Radiative Transfer* (New York: Dover)
- Chauvin, G., Lagrange, A.-M., Dumas, C., Zuckerman, B., Mouillet, D., Song, I., Beuzit, J.-L., & Lowrance, P. 2004, *A&A*, 425, L29
- Cushing, M. C. et al. 2008, *ApJ*, 678, 1372
- Fluri, D. M., & Stenflo, J. O. 1999, *A&A*, 341, 902
- Freedman, R. S. et al. 2008, *ApJS*, 174, 71.
- Han, C., Jung, Y. K., Udalski, A., et al. 2013, *ApJ*, 778, 38
- Harrington, J. P. 1969, *AstrophysJ*, 3, 165
- Joergens, V., & Muller, A. 2007, *ApJL*, 666, L113
- Jensen-Clem, R, Millar-Blanchaer, M, Mawet, D. et al. 2016, *ApJ* (in press) eprint arXiv:1601.01353
- Kirkpatrick, J. D. 2005, *ARA&A*, 43, 195.
- Kostogryz, N. M., Yakobchuk, T. M., Morozhenko, O. V., & VidMachenko, A. P. 2011, *MNRAS*, 415, 695

- Liu, Q. & Weng, F. 2006, *Applied Optics*, 45, 7475.
- Marley, M. S. & Robinson, T. D., 2015, *ARA&A*, 53, 279
- Marley, M. S. & Sengupta, S. 2011, *MNRAS*, 417, 2874
- Marley, M. S. et al. 2002, *ApJ*, 568, 335.
- Menard, F. et al. 2002, *A&A*, 396, L35
- Miles-Pez, P. A., Zapatero Osorio, M. R., Pall, E., & Pea Ramirez, K. 2013, *A&A*, 556, 125
- Saumon, D., & Marley, M. S. 2008, *ApJ*, 689, 1327
- Scharf, C. A. 2009, *Extrasolar Planets and Astrobiology*, Chapter 9 (University Science Books : Sausalito, California).
- Sengupta, S. & Krishan, V. 2001, *ApJ*, 561, L123
- Sengupta, S. 2003, *ApJ*, 585, L155.
- Sengupta, S. & Kwok, S. 2005, *ApJ*, 625, 996.
- Sengupta, S. & Marley, M. S. 2009, *ApJ*, 707, 716
- Sengupta, S. & Marley, M. S. 2010, *ApJL*, 722, L142
- Sengupta, S. & Marley, M. S. 2016, *ApJ* (in press), eprint arXiv:1604.04773.
- Snellen, I. A. G., Brandl, B. R., de Kok, R. J., Brogi, M., Birkby, J. & Schwarz, H., 2014, *Nature*, 509, 63
- Stephens, D. C. et al. 2009, *ApJ*, 702, 154
- Tata, R. et al. 2009, *A&A*, 508, 1423.
- Todorov, K., Luhman, K. L., & McLeod, K. K. 2010, *ApJL*, 714, L84
- Udalski, A., Jung, Y. K., Han, C. et al. 2015, *ApJ*, 812, 47
- Wiktorowicz, S. J., & Laughlin, G. P. 2014, *ApJ*, 795, 12
- Zapatero Osorio, M. R., Caballero, J. A., & B ejar, V. J. S. 2005, *ApJ*, 621, 445
- Zapatero Osorio, M. R., B ejar, V. J. S., Goldman, B., et al. 2011, *ApJ*, 740, 4

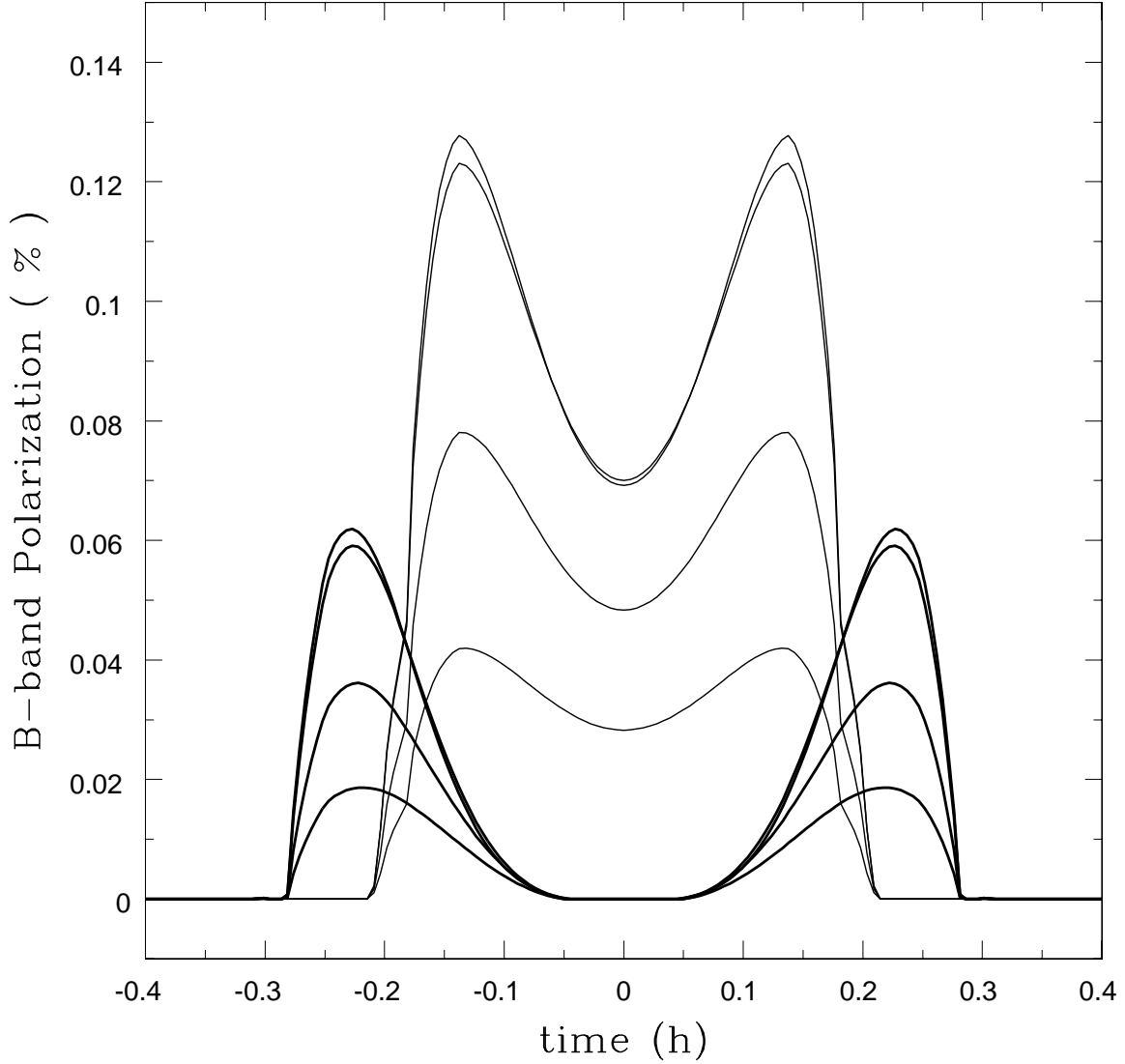


Fig. 1.— Disk integrated B-band polarization of T-dwarfs during the transit of an exoplanet. From top to bottom, the thick and thin solid lines represent T-dwarf models with $T_{eff} = 700, 900, 1100$ and 1300 K respectively. The thick solid lines represent models for an Earth-size transiting planet with 90° orbital inclination angle and the thin solid lines represent models for transiting exoplanet with radius $3R_\oplus$ and inclination angle 89° . For all cases, the radius of the T-dwarf is set to $1R_J$ and $g=1000 \text{ ms}^{-2}$. The orbital distance of the exoplanet is 0.01 AU .

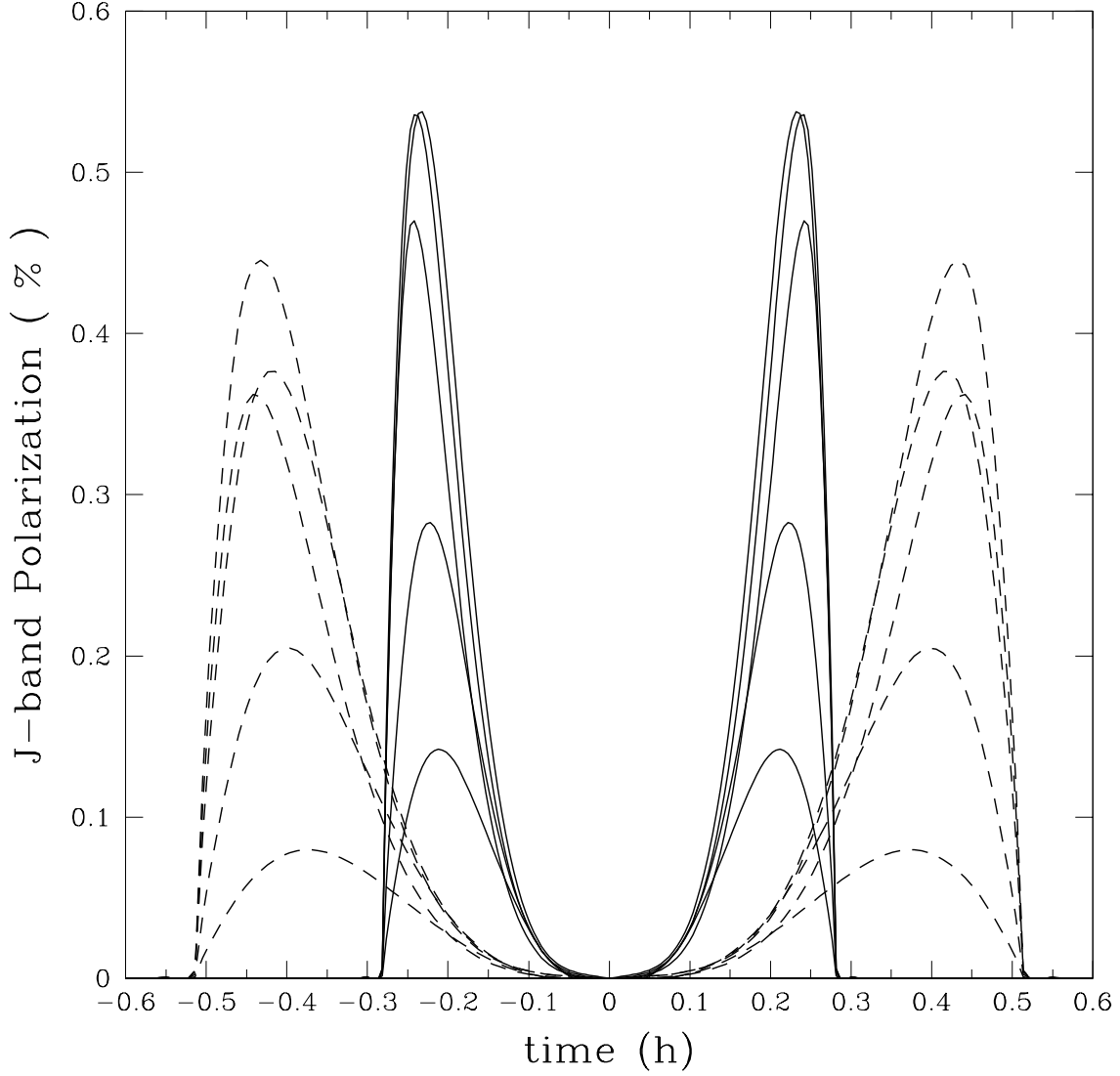


Fig. 2.— Disk integrated J-band polarization of a cloudy L-dwarfs during the transit of an Earth-size planet with orbital inclination angle $i = 90^\circ$ and orbital distance $a = 0.01$ AU. Solid lines represent L-dwarf with surface gravity $g=1000 \text{ ms}^{-2}$ and dashed lines represent L-dwarf with $g=300 \text{ ms}^{-2}$. From top to bottom the lines represent L-dwarfs with $T_{eff} = 1600, 1800, 1400, 2000$ and 2200 K respectively.

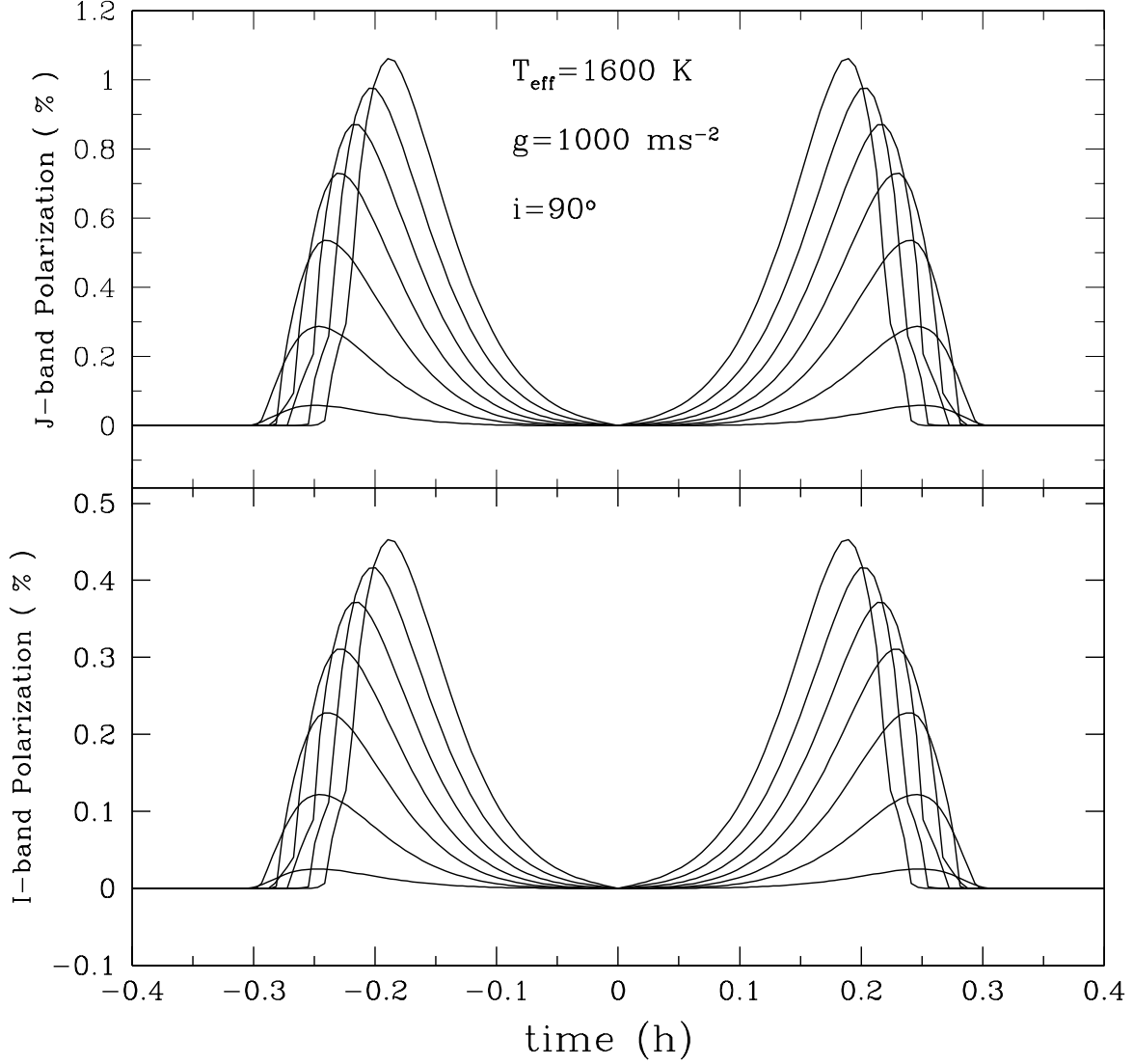


Fig. 3.— Disk integrated J- and I-band polarization of a L-dwarf with $T_{eff} = 1600\text{K}$ and $g=1000\text{ ms}^{-2}$ during the transit of exoplanets with different sizes but with a fixed orbital inclination angle $i = 90^\circ$ and orbital distance $a = 0.01\text{ AU}$. In both the panels, the solid lines from top to bottom represent polarization by transiting exoplanet of radius 0.1, 0.5, 1.0, 1.5, 2.0, 2.5 and $3.0 R_\oplus$ respectively where R_\oplus is the radius of the Earth.

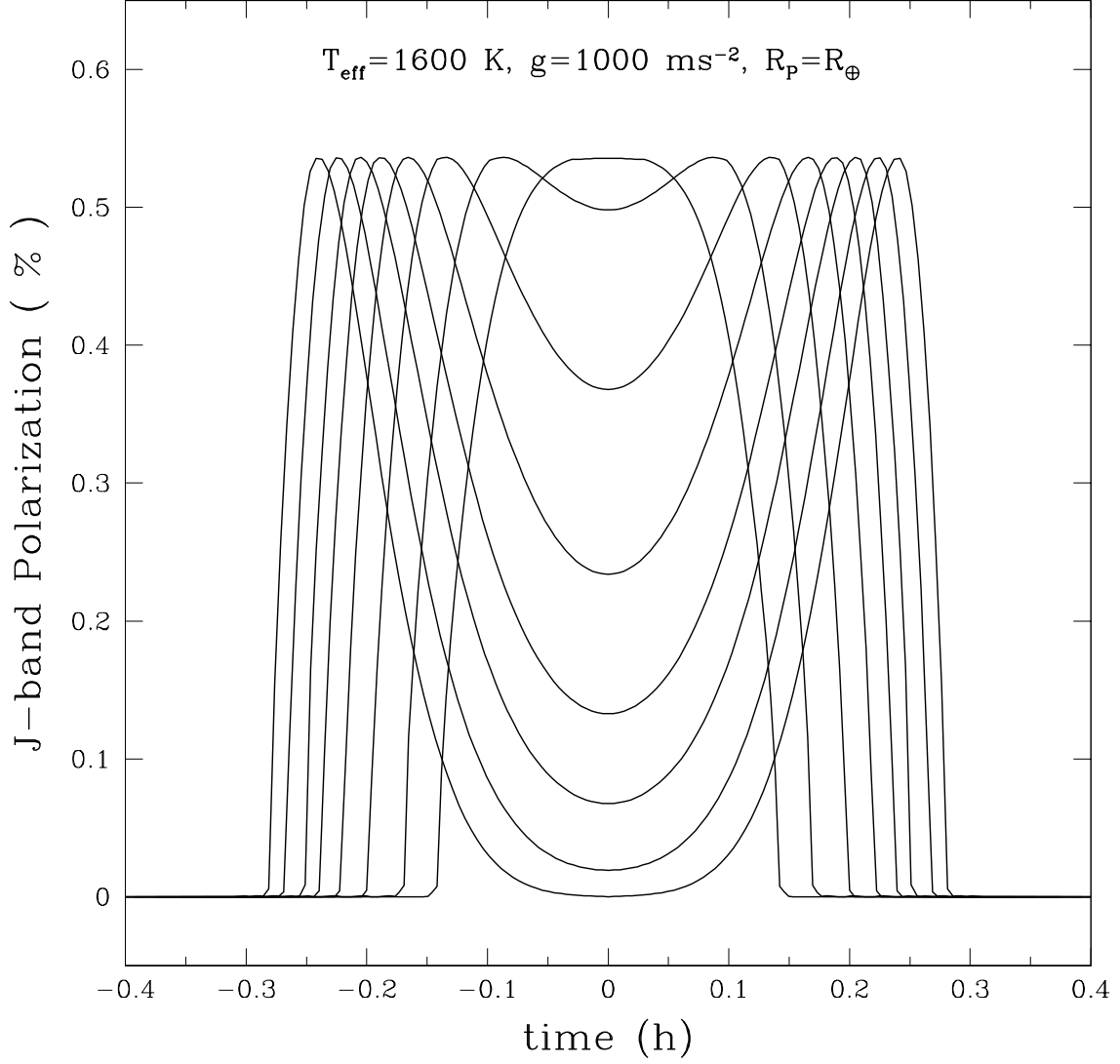


Fig. 4.— Disk integrated J-band polarization of a L-dwarf with $T_{\text{eff}} = 1600\text{K}$ and $g=1000 \text{ ms}^{-2}$ during the transit of an Earth-size planet orbiting at a distance of 0.01 AU but with different orbital inclination angles. From bottom to top at 0 h, the solid lines represent models with $i=90.0, 89.3, 89.0, 88.8, 88.6, 88.4, 88.2$ and 88.0° respectively.